Elsevier Editorial System(tm) for Nuclear Inst. and Methods in Physics Research, A
Manuscript Draft

Manuscript Number: NIMA-D-18-00758

Title: Neutron Response Functions of Superheated Droplet Detectors

Article Type: Full length article

Section/Category: Space Radiation and Underground Detectors

Keywords: superheated liquids, neutron detectors, Monte Carlo

Corresponding Author: Dr. Ana C Fernandes, Ph.D.

Corresponding Author's Institution:

First Author: Ana C Fernandes, Ph.D.

Order of Authors: Ana C Fernandes, Ph.D.; Tomoko A Morlat, Ph.D.; Andreas Kling, PhD; Maxime Lamotte, MSc; Miguel Felizardo, PhD; Carlos Cruz, PhD

Abstract: The response functions of various C2ClF5 superheated droplet detectors fabricated by our team were calculated using the MCNPX-PoliMi and GEANT4 Monte Carlo radiation transport simulation codes. The simulation approach was validated by measurements using an Am-Be source.

Neutron Response Functions of Superheated Droplet Detectors

A.C. Fernandes[1,*], T.A. Morlat[1], A. Kling[1], M. Lamotte[1], M. Felizardo[1], C. Cruz[2]

[1]Centro de Ciências e Tecnologias Nucleares (C[2]TN), Instituto Superior Técnico, Universidade de Lisboa

Campus Tecnológico e Nuclear, E.N. 10 (km 139.7), 2695-066 Bobadela, Portugal

[2]Instituto de Plasmas e Fusão Nuclear (IPFN), Instituto Superior Técnico, Universidade de Lisboa

Campus Tecnológico e Nuclear, E.N. 10 (km 139.7), 2695-066 Bobadela, Portugal

*Corresponding author: anafer@ctn.tecnico.ulisboa.pt

Abstract

The response functions of various C_2ClF_5 superheated droplet detectors fabricated by our team were calculated using the MCNPX-PoliMi and GEANT4 Monte Carlo radiation transport simulation codes. The simulation approach was validated by measurements using an Am-Be source.

Keywords: superheated liquids, neutron detectors, Monte Carlo

1. Introduction

Superheated liquids are employed as radiation detectors by identifying the vaporization of the liquid following energy absorption from radiation. A superheated droplet detector (SDD) is an emulsion of micrometric superheated droplets in a gel matrix that reduces the occurrence of spontaneous nucleations. The physics underlying SDD operation are summarized in Refs. 1 and 2: radiation-induced nucleations are subject to a dual threshold condition regarding the energy deposited within the droplet and the deposition distance along the particle track, i.e., the radiation linear energy transfer (LET). The overall critical energy necessary to induce a nucleation (E_c) is found to depend on the liquid and on the operation thermodynamic conditions. By operating at reduced superheat (slightly above boiling conditions) the SDD can be rendered insensitive to minimum ionizing particles (mip). In these conditions, at terrestrial levels the SDD is only sensitive to nuclear recoils following neutron interactions and to alpha particles (α) that originate from embedded emitters. These can be further discriminated on the basis of the acoustic signal amplitudes, α's inducing larger amplitudes due to the production of various proto-bubbles [3]. The intrinsic insensitivity to mip's and the n/α discrimination are crucial to the low neutron-induced noise of the SDD.

Superheated droplet detectors developed by our team at C^2TN have been employed in rare event experiments at underground facilities [4]. The characterization of the detectors' signal induced by the environmental neutron background is crucial for the analysis of measurements. This task often relies on calculation tools and facility models, as the extremely low intensity of the neutron environment hinders most experimental approaches.

With SDDs being conventionally used for neutron spectrometry at irradiation facilities, as well as individual and ambient dose measurements [2], the present work focuses on their application in various low neutron intensity frameworks. Calculations and measurements of the intrinsic signal of 1L detectors (containing ~14 g C_2ClF_5) have yielded a neutron-induced noise level of ~6×10^{-3} events per day, corresponding to a fast neutron fluence rate detection limit smaller than 10^{-7} cm^{-2} s^{-1} [5]. The devices can be therefore operated as low-noise neutron detectors particularly fit for neutron measurements in massively shielded facilities. With boiling and critical points lower than most liquids, C_2ClF_5 SDDs can be employed on neutron measurements down to 10-100 keV and in the thermal energy range [2]. Their neutron response functions are herein investigated via Monte Carlo radiation transport simulation.

2. Materials and Methods

2.1 Detectors

This work is focused on 1-3 wt.% C_2ClF_5 SDDs; details on devices fabrication and acoustic instrumentation can be found in Ref. 4 and references therein. Detector volumes (Fig. 1) were: (i) 1 L (85x85 mm cross section) employed in astrophysics experiments; (ii) 150 mL (∅ 60 mm circular cross section) standard test prototypes, and (iii) 4 mL (∅ 13 mm) devices for cell irradiation dosimetry.

Figure 1. The evaluated C_2ClF_5 devices.

2.2 Measurements

The dependence of E_c on the thermodynamic conditions yields the possibility to perform neutron spectrometry by changing the operation temperature (T) and/or pressure (p). In this work, the response of a 150 mL SDD (1.6 g liquid) to Am-Be neutrons was measured as a function of T (from 4 to 13 ºC) at 2 bar. Superheated liquids are employed as radiation detectors by identifying the vaporization of the

The set-up sought to accumulate less than 10^3 bubbles during the experiment - beyond which the biphasic medium induces a noticeable degradation of the acoustic signal. The neutron source (∅17 x 19 mm) with 0.09 mCi activity was placed at a distance of 1.5 m from the SDD. The test SDD was placed in a small thermostatic water bath (yielding a layer of 2 cm water around the SDD) and covered with aluminum foil to reduce air convection. A dummy SDD (without liquid) was used to monitor the detector temperature. The devices were left to stabilize for 1 hour following any temperature change. The test SDD is pressurized at 2 bar prior to each measurement in order to compensate potential pressure drops. Each measurement ran for 60 min. Background measurements were also performed.

2.3 Monte Carlo simulations

Neutron response functions of SDDs are usually calculated with general-purpose radiation transport Monte Carlo simulation codes. Studies using MCNP [6] consider homogenized droplet+matrix materials and are coupled to energy deposition data processing codes, whereas GEANT is very convenient to discriminate and simulate the energy absorption within the droplets [1]. In this work, the MCNPX-PoliMi code was employed, with MNCPX (v.2.7.0) simulating the neutron transport and MCNPX-PoliMi (v.2.0) extracting the corresponding recoil distributions. The GEANT4 code (v.10.3–p.01) with the neutron high precision (HP) model from the QGSP_BERT_HP physics was also used to calculate both neutron and recoil distributions - to be compared with the MCNPX-PoliMi results. Stopping power tables of Ziegler/SRIM were used to derive E_c.

Material compositions and densities were taken from Ref. 4. An homogeneous liquid-gel mixture [6] with 10 wt.% liquid was considered. The liquid concentration is increased relative to the real SDD in order to reduce the statistical uncertainty in the recoil distribution retrieval. The atomic concentration of hydrogen - the main gel ingredient, followed by oxygen - is diminished by only 2% (from 58.4% at 1 wt.% liquid) yielding a negligible systematic error on the calculated detector signal.

Neutron fluence rates (track length estimator) and recoil distributions in the detector volume were determined as a function of the incident neutron energy. For the calculation of response functions, monoenergetic, monodirectional plane neutron sources at 10 cm from the SDD axis were considered. The simulation of the Am-Be irradiation assumed a point isotropic source at 1.5 m from the SDD. The neutron energy spectrum was extracted from the ISO-8529-1:2001 standard. The data (in the 10^{-7}-10 MeV energy range) refers to an emission undisturbed by the source structure hence underestimates the low energy region of the spectrum. Neutron interactions within the experimental set-up were neglected except for the thermostatic SDD bath included in the model. The results were scaled per neutron incident on the detector surface and per unit mass of liquid when applicable.

3. Results and Discussion

3.1 Neutron fluence

The energy distribution of the on-detector neutron fluence rates (Fig. 2) shows the modification exerted by the SDD over the incident neutron spectrum, with a downscatter region that, for the larger volume devices (150 mL and 1 L), terminates in a thermal neutron peak. The discrepancy between GEANT4- and MCNPX-calculated neutron fluence rates is smaller than 7% for all neutron energies and within 1-2% for neutron energies larger than 1 eV and for the total neutron fluence rate. This result is similar to that of other works using the GEANT4 HP models [7].

Fig.2. On-detector neutron fluences.

3.2 Event-producing reaction rates

Among the various reaction channels available the predominant event-producing reactions in C_2ClF_5 (for the neutron energy, T and p ranges considered) are elastic and inelastic scattering with the droplet atoms and the exoergic (n,p) and (n,α) reactions in ^{35}Cl [6]. The case of ^{16}O was evaluated as a potential contributor from the gel to the detector signal (hydrogen does not reach the LET required for a nucleation).

Values of E_c for the reaction products are represented in Fig. 3. The results show that E_c is reduced with increasing T and lower p, i.e. smaller heat spikes can trigger a nucleation as the liquid T exceeds its boiling temperature at pressure p. The situation is clearly represented by the E_c(T) curves for Cl and S, which fulfill the dual threshold nucleation condition once their energy overcomes the constraint on the droplet-deposited energy. The scenario is modified for lighter nuclei, where the LET restriction is not fulfilled in the overall temperature range, yielding a distinctive LET-defined regime at low T with a sharp transition to the common, E-defined curve. The "knee" is shifted to higher temperature as the nucleus mass is reduced.

Fig. 3. Critical recoil energy of C_2ClF_5 atoms as a function of p and T.

The neutron energy transfer to the recoils, determined by the reaction kinematics equations, is the product of the maximum energy transferred and an angular factor. For elastic scattering, the minimum neutron energy required to induce a nucleation (E_{min}) is directly proportional to E_c and therefore varies with T, p for each atom of the liquid. In contrast, the energy of nuclei emerging from $^{35}Cl(n,p)^{35}S$ (17 keV) and $^{35}Cl(n,\alpha)^{32}P$ (104 keV) is always sufficient to provoke an event at $T \geq 2$ °C with ^{35}S being the main trigger at low neutron energies [2, 6].

The various excited states induced by inelastic scattering were analyzed individually for $T \geq 4$ °C. At p=1 bar all states induce events, except the first excited state of ^{19}F with a small threshold energy (115.84 keV) that always provokes a nucleation if $T \geq 2$ °C. At 2 bar the same generally applies: all emerging states of $^{35/37}Cl$, $^{12/13}C$ and ^{19}F contribute beyond 4-7 °C while T-dependent thresholds apply for the first excited state of ^{19}F up to 11 °C.

The energy distributions of reaction rates are plotted in Fig. 4, in which the part above E_{min} indicates the event-producing region. The sharp features found in the 10-100 keV range correspond to the resonances in the $_{19}F$ elastic scattering cross section – the largest contributor to the detector signal at T>8 °C (2 bar) for neutron energies larger than a few tens of keV .

Fig. 4. Reaction rate of neutron scattering reactions.

3.3 Recoil distributions

Figure 5 shows calculated energy distributions of recoils, and the E_c corresponding to elastic scattering at 9 °C and 2 bar (similarly to Fig. 4). The inclusion of the angular distribution of recoils is found to reduce the calculated event rate by 10-20% relative to estimates assuming maximum energy transfer. MCNPX-PoliMi and GEANT4 recoil distributions are in good agreement at energies higher than 1-10 keV.

Fig. 5. Recoil energy distributions (C+F+Cl).

3.4 Response functions

Detector responses as a function of energy (for fixed T and p) and as a function of T (for fixed energy and p) are shown in Fig. 6, and exhibit the general features reported in the literature [1, 2, 6] for similar values of superheat. The energy dependence corresponds to the convolution of the reaction rate above E_{min} with the recoil distribution (Figs. 4 and 5). Some resonant features of the elastic scattering in ^{19}F are retained once T is sufficiently high to embark their energy region. The temperature dependence is similar to a threshold response curve, due to the features discussed in Fig. 3. The base level and the two kinks in the response display the contribution of the Cl, F and C recoils.

Fig. 6. Detector response functions. Top: energy dependence (2 bar). Bottom: T dependence (1 MeV neutrons).

3.5 Comparison with measurements

The calculated and measured responses as a function of temperature of a 150 mL SDD at p=2 bar irradiated with Am-Be are shown in Fig. 7. The measurement uncertainties correspond to counting statistics. There is a fast rise in the detector signal with T due to the threshold-like character of the response curve, followed by a plateau as the whole neutron energy range triggers nucleations. The measurements follow generally the calculated distribution curve and the expected count rate. Discrepancies can be explained by the actual neutron energy, room scattering and the simulation process – the code accuracy contributing with 10% uncertainty.

Fig. 7. Measured and calculated responses as a function of T for Am-Be neutrons.

4. Conclusions

The neutron response functions of the various C_2ClF_5 SDDs fabricated by our team were calculated for the first time using Monte Carlo radiation transport simulation. The calculated response functions exhibit the characteristics found by other authors. The response measured as a function of temperature for Am-Be neutrons follows the calculated shape and intensity. GEANT4 provided results in good agreement with those of MCNPX-PoliMi with respect to neutrons of all energies and to recoils beyond 1-10 keV. We look forward for a revised GEANT4 release that accounts properly for the transport of low energy recoils, allowing to model the energy deposition process of the liquid and gel atoms within the micrometric droplets. The improved simulation of the detector response is planned for the near future, followed by benchmarking measurements using monoenergetic neutrons.

5. Funding

This work received funding from projects IF/00628/ 2012/CP0171/CT0008 and PTDC/EEI-ELC/2468/ 2014 of the Portuguese Foundation for Science and Technology (FCT). Activities were also supported by FCT via grant SFRH/BPD/94028/2013, project UID/ Multi/04349/2013 and contract IF/00628/2012.

6. References

[1] M. Barnabé-Heider, M. Di Marco, P. Doane, et al., Response of superheated droplet detectors of the PICASSO dark matter search experiment, Nucl. Instrum. Meth. A 555 (2005) 184-204.

[2] F. d'Errico, Radiation dosimetry and spectrometry with superheated emulsions. Nucl. Instrum. Meth. B 184 (2001) 229-254.

[3] M. Felizardo, T. Morlat, A. Kling, et al., Neutron-Alpha irradiation response of superheated emulsion detectors, Nucl. Instrum. Meth. A 863 (2017) 62-73.

[4] M. Felizardo, T.A. Girard, T. Morlat, et al., The SIMPLE Phase II dark matter search. Phys. Rev. D 89 (2014) 072013.

[5] A.C. Fernandes, T.A. Morlat, M. Felizardo, et al., Intrinsic noise of a superheated droplet detector for neutron background measurements in massively shielded facilities. EPJ Web of Conferences 153 (2017) 07013.

[6] G.F. Gualdrini, F. d'Errico, P. Noccioni, Monte Carlo evaluation of the neutron efficiency of a superheated droplet detector (Ente per le Nuove Tecnologie, l'Energia e l'Ambiente, Bologna, Italy), ENEA RT/AMB/97/1, 1997.

[7] B.M. van der Ende, J. Atanakovich, A. Erlandson, et al., Use of GEANT4 vs. MCNPX for the characterization of a boron-lined neutron detector, Nucl. Instrum. Meth. A 820 (2016) 40-47.

Figure Captions

Figure 1. The evaluated C_2ClF_5 devices. From left to right: 4 mL SDD and microphone; 150 mL SDD with a modified cap to embed the signal and pressure feedthroughs (note the microphone embed in a glycerin layer covering the translucent emulsion); 1 L SDD displaying gel fractures after exposure to high fast neutron fluence.

Figure 2. On-detector neutron fluences. The smooth line represents a GEANT4 calculation (150 mL, 10 MeV).

Figure 3. Critical recoil energy (E_c) of C_2ClF_5 atoms as a function of p and T.

Figure 4. Reaction rate of neutron scattering reactions. The solid circles and stars identify E_{min} for elastic scatterings at 7 ^oC and 9 ^oC (2 bar), respectively.

Figure 5. Recoil energy distributions (C+F+Cl). The smooth line represents a GEANT4 calculation (150 mL, 10 MeV).

Figure 6. Detector response functions. Top: energy dependence (2 bar). Bottom: T dependence (150 mL SDD, 1 MeV neutrons except when indicated otherwise).

Figure 7. Measured (circles) and calculated (lines) response as a function of T for Am-Be neutrons.

Figure 1. The evaluated C_2ClF_5 devices. From left to right: 4 mL SDD and microphone; 150 mL SDD with a modified cap to embed the signal and pressure feedthroughs (note the microphone embed in a glycerin layer covering the translucent emulsion); 1 L SDD displaying gel fractures after exposure to high fast neutron fluence.

Figure 2. On-detector neutron fluences. The smooth line represents a GEANT4 calculation (150 mL, 10 MeV).

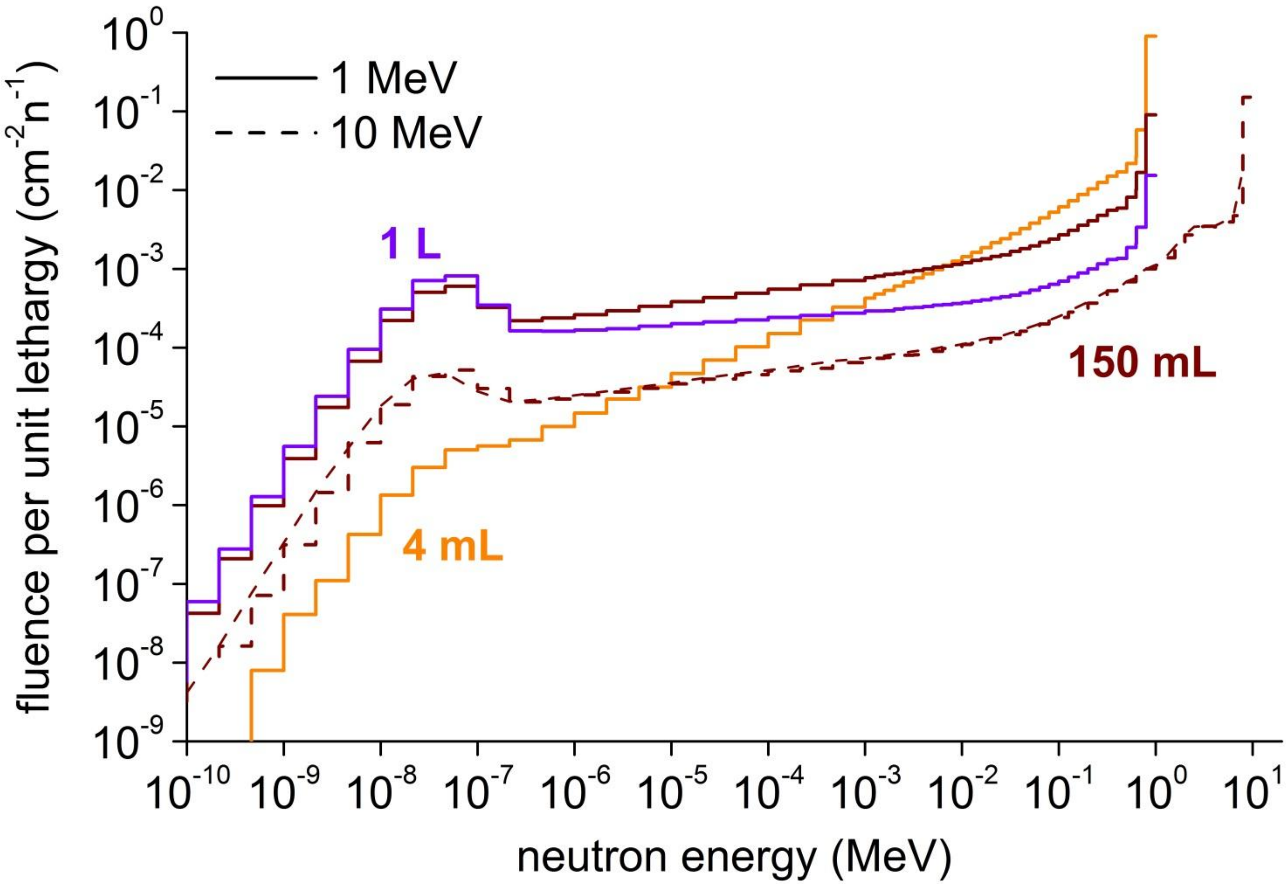

1 **Figure 3.** Critical recoil energy (E_c) of C_2ClF_5 atoms as a function of p and T.

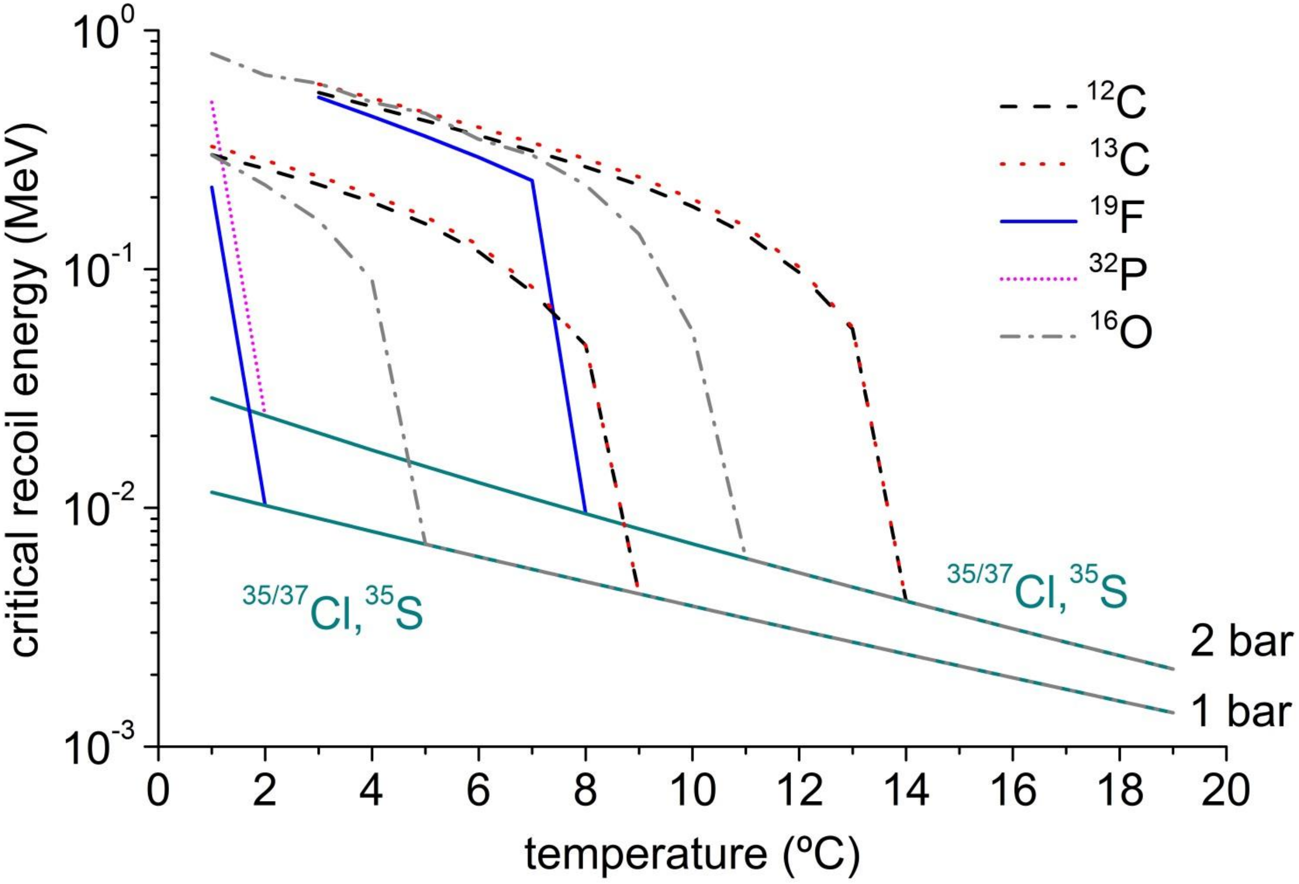

2

Figure 4. Reaction rate of neutron scattering reactions. The solid circles and stars identify E_{min} for elastic scatterings at 7 ^{o}C and 9 ^{o}C (2 bar), respectively.

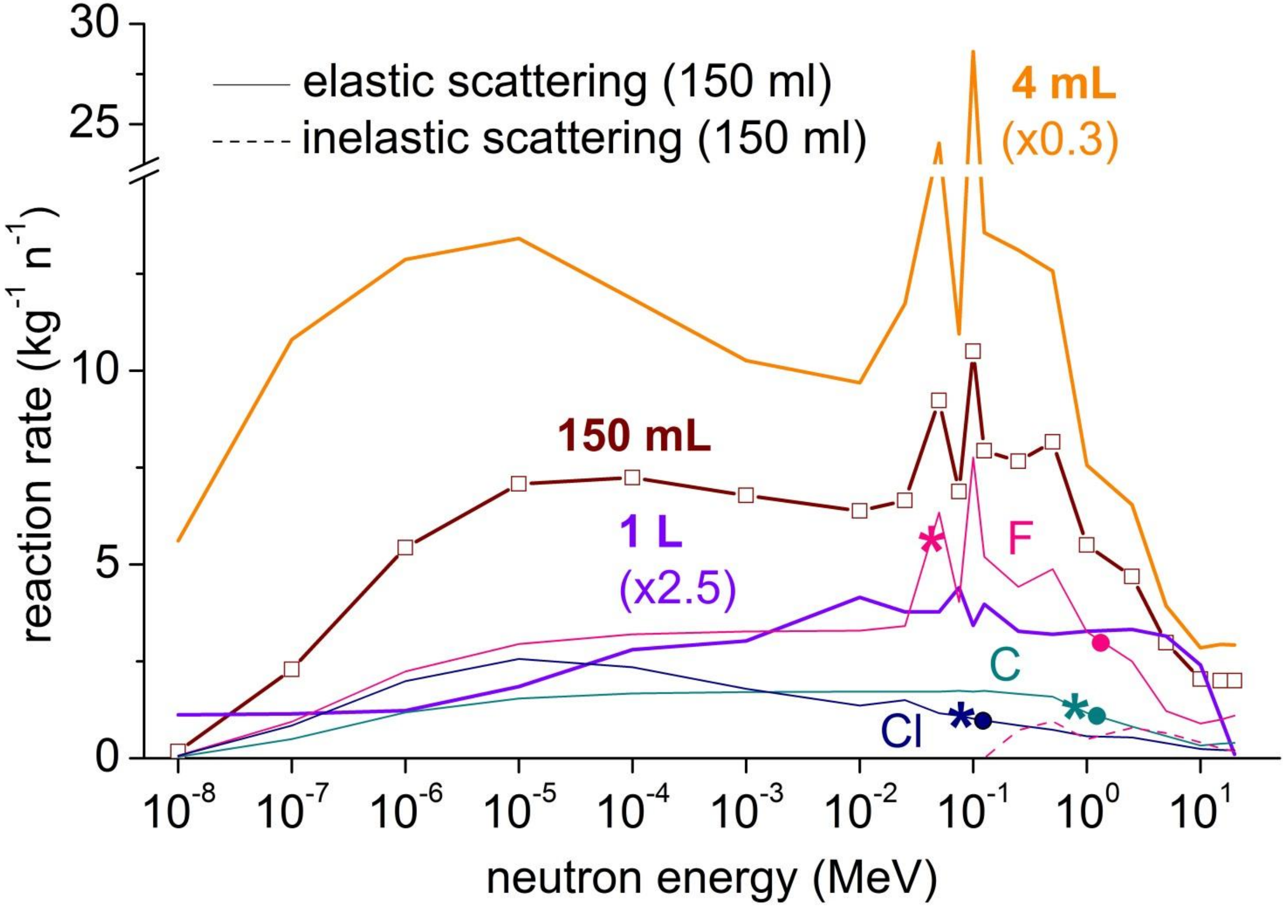

Figure 5. Recoil energy distributions (C+F+Cl). The smooth line plots a GEANT4 calculation (150 mL, 10 MeV).

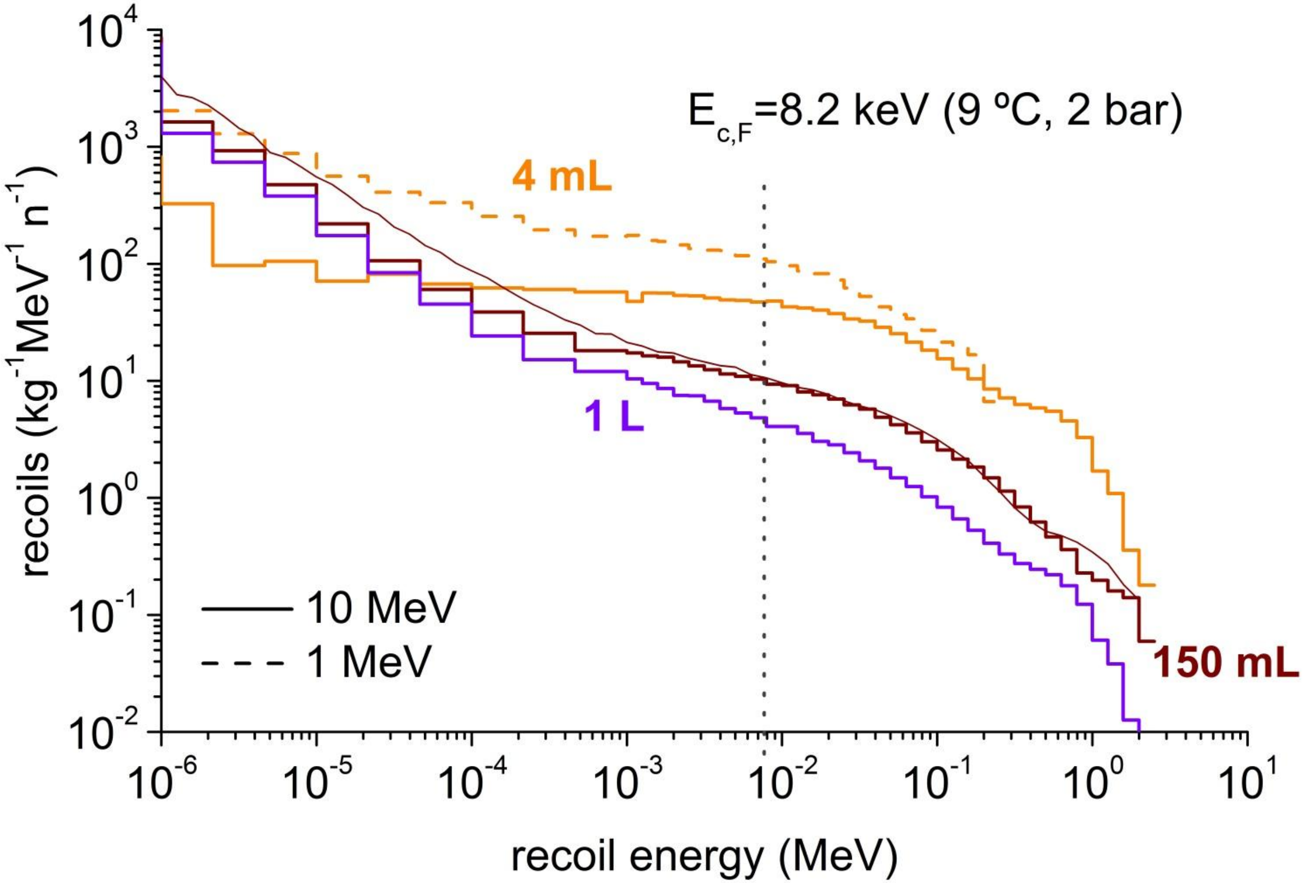

Figure 6. Detector response functions. Top: energy dependence (2 bar). Bottom: T dependence (150 mL SDD, 1 MeV neutrons except when indicated otherwise).

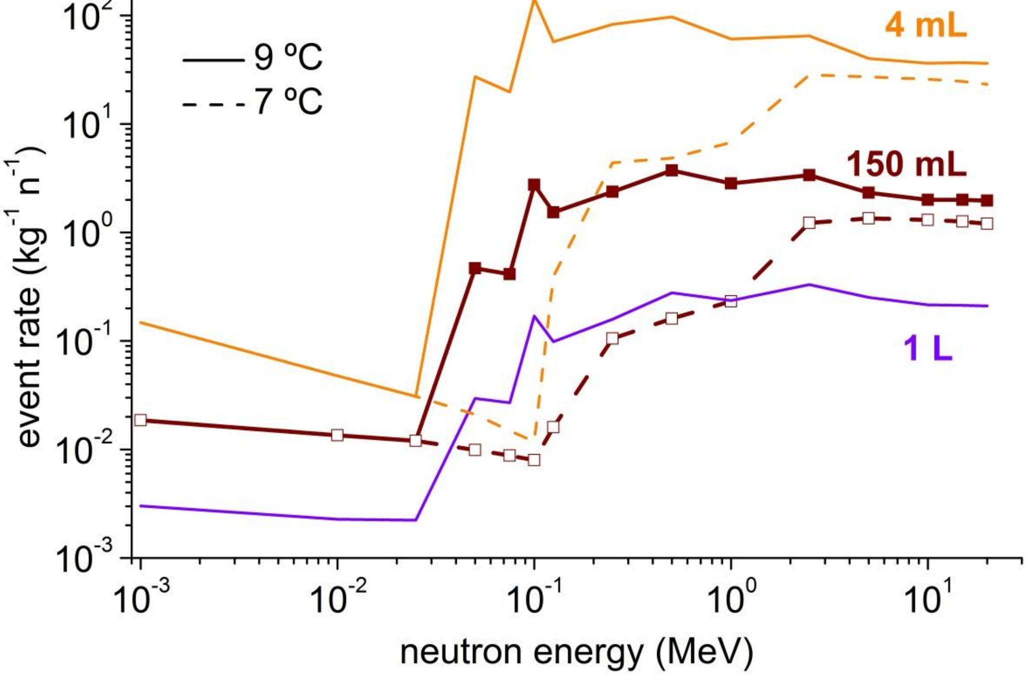

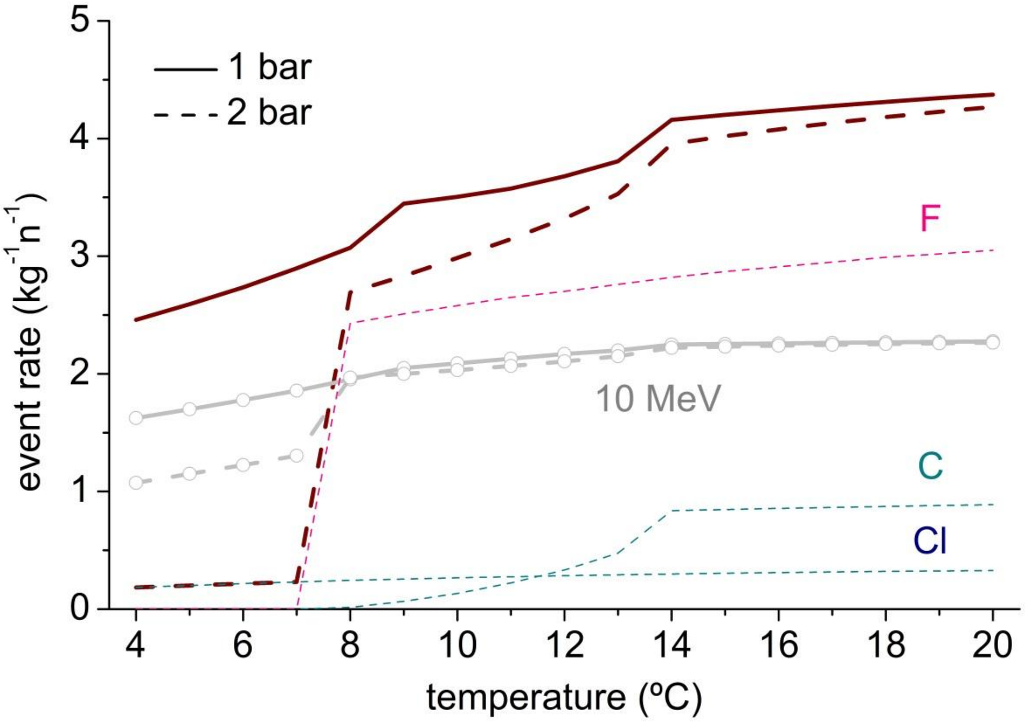

1 **Figure 7.** Measured (circles) and calculated (lines) response as a function of T for Am-Be neutrons.

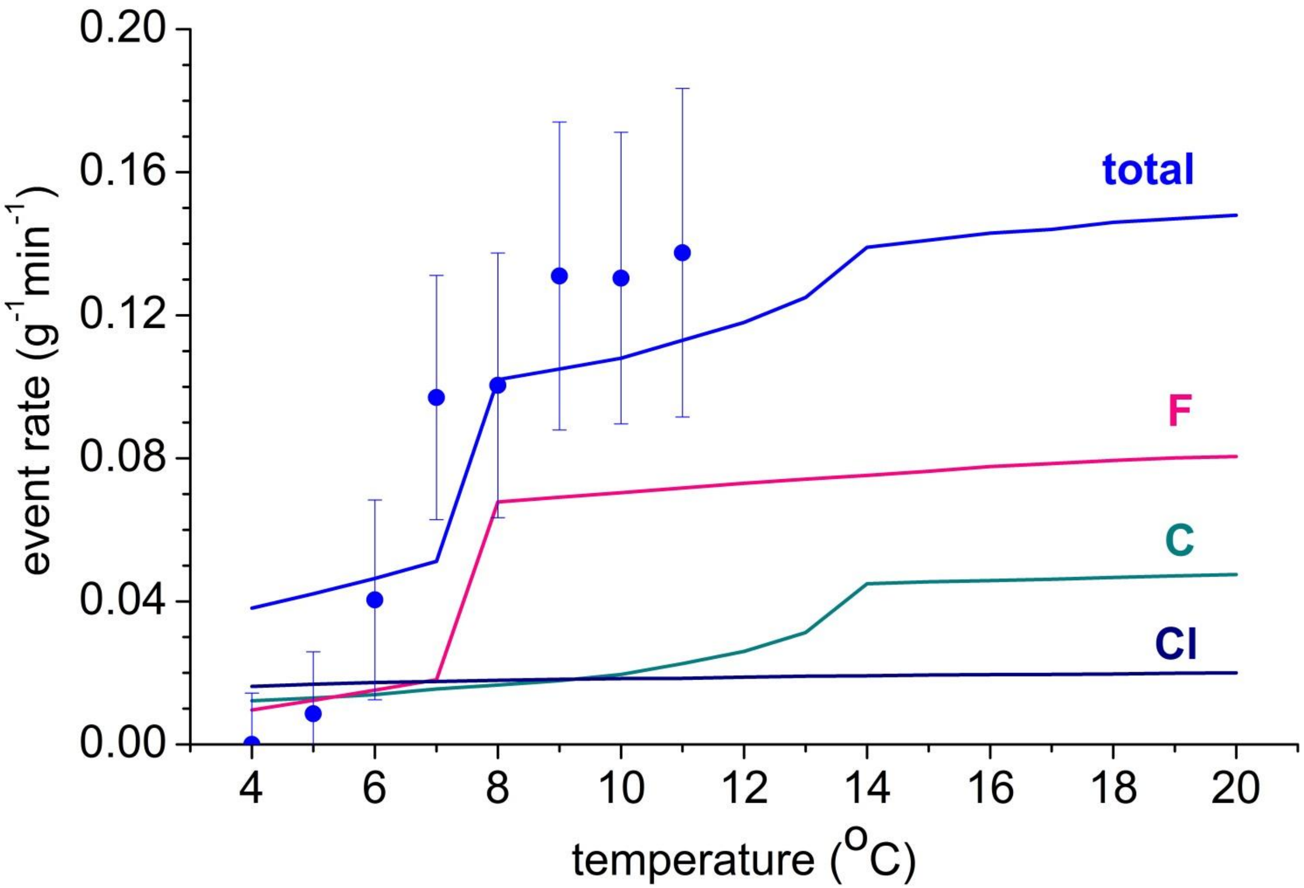

2